Laser Physics, Vol. 8, No. 1, 1998, pp. 47–55.

Nonstationary Effects in Laser Ablation of Indium: Calculations Based on Spatial Moments Technique

N. Arnold*, B. Luk'yanchuk, N. Bityurin***, and D. Bäuerle***

** Angewandte Physik, Johannes Kepler Universität Linz, Linz, A-4040 Austria*
e-mail: nikida.arnold@jk.uni-linz.ac.at
e-mail: dieter.baeuerle@jk.uni-linz.ac.at
*** General Physics Institute, Russian Academy of Sciences, Moscow, 117942 Russia*
e-mail: lukyanch@kapella.gpi.ru
**** Institute of Applied Physics, Russian Academy of Sciences, Nizhnii Novgorod, 603600 Russia*
e-mail: bit@appl.sci-nnov.ru
Received August 7, 1997

Abstract—The nonstationary averaging technique (spatial moments technique) is used for the solution of nonlinear heat equation describing laser ablation. The temperature dependencies of material parameters and the temporal profile of laser beam are taken into account. Nonstationary heat equation is reduced to three ordinary differential equations for the surface temperature, spatial width of the enthalpy distribution, and the ablated depth. Calculations have been done for laser ablation of indium, where we study the influence of the duration and temporal profile of the laser pulse on the threshold fluence, Φ_{th}, the influence of temperature dependencies in material parameters on the overall ablation kinetics (ablated depth versus laser fluence), the duration of the surface melt presence, etc.

1. INTRODUCTION

Laser ablation is used in many technological applications like micropatterning (for microelectronics, micromechanics, etc.), pulsed laser deposition including multilayer structures with atomic thickness, like X-ray mirrors, formation of nanoclusters, etc. [1–4].

To optimize these applications it is important to understand the fundamental aspects of laser–matter interaction. The coupling mechanisms of the laser light to the ablated sample can be very complex. They are related to the change of thermophysical and optical characteristics during laser heating, phase transitions, hydrodynamic effects, absorption of radiation within the plume, optical breakdown of vapor, plasma formation etc. Many of these effects are accompanied by numerous instabilities [5]. It is clear that there are no simple analytical formulas which can be easily applied to a given experimental situation.

The situation becomes even more complex for ultrashort (subpicosecond) laser pulses where nonlinear absorption, critical phenomena, different temperatures of electron gas and lattice come into play [5]. Meanwhile, shorter laser pulses are used to produce better ablation characteristics.

To analyze numerous effects in laser ablation, both, the experimental investigations and the theoretical simulations are needed. For the effective feedback between theory and the experiment one should develop semianalytical methods of "intermediate power," which should be flexible, applicable for quantitative analysis of experimental data and can be done within seconds on a PC. Now there is a big gap between the primitive theoretical analysis related to the solution of the linear heat equation and direct numerical solution of nonlinear heat equation (or hydrodynamics equations) by finite-differences or finite-elements technique with the help of powerful computers. In the first case the analysis is oversimplified and cannot be used sometimes even for qualitative consideration. In the second case the analysis refers to some particular problems and is not flexible, one cannot apply this technique for a fast analysis of experimental data.

The first question which should be clarified during the analysis is related to the ejection mechanism: is it purely thermal surface vaporization, or do other mechanisms (hydrodynamics, nonequilibrium excitation of electrons, phonons, etc.) contribute to the ejection? The lack of real quantitative analysis of experimental data in the broad range of parameters (especially in the field of polymer ablation) leads to many speculations and discussions. It is especially important for short laser pulses where new effects are expected during the transition from nanosecond to femtosecond ablation regime. The border for these effects lies probably in the subpicosecond range and depends on the material.

In the present paper we applied the nonstationary averaging (moments technique) to solve the nonlinear heat equation, where one takes into account

– arbitrary *temperature dependencies* of material parameters, such as the specific heat, thermal conductivity, absorptivity, absorption coefficient, etc.;

– arbitrary *temporal profiles* of the laser pulse;

– strong (Arrhenius-type) dependence of the ablation velocity on the temperature of the ablation front, which leads to a *nonsteady movement* of the ablation boundary during the (single) pulse;

– *screening* of the incoming radiation by the ablated product;

– influence of the ablation (vaporization) enthalpy on the heating process;

– influence of melting and/or other phase transformations.

Not included are hydrodynamic effects, nonlinear optical effects, optical breakdown, nonequilibrium distribution in the lattice and electron gas, and thermally induced stresses.

Calculations have been done for laser ablation of indium. Here, thermal properties change strongly below and at the melting point. At the same time (apart from absorption coefficient, which behavior is difficult to estimate) they are almost constant at elevated temperatures. Calculations have been done for the radiation with 248 nm (KrF excimer laser) where the experimental data on subpicosecond laser ablation were published recently [6]. We study the influence of the duration and temporal profile of the laser pulse on the threshold fluence, Φ_{th}, the influence of temperature dependencies in material parameters on the overall ablation kinetics (ablated depth versus laser fluence), the duration of the surface melt presence, etc. At higher fluences one can expect the change in ablation kinetics related to hydrodynamic effects (for nanosecond ablation) and to the critical phenomena (for picosecond ablation regime).

2. THE MODEL

For the analysis of laser ablation process the following approximation is often used. It is assumed that after a certain delay time the ablation proceeds (quasi) stationary i.e., with constant ablation velocity v. The delay time is found from the nonstationary heat equation with $v = 0$ [1, 5, 7, 8]. In reality, one should solve the *nonstationary* heat conduction problem with $v = v(t)$ for all times. An accurate description of nonstationary effects in ablation and nonlinearities related to temperature dependencies of parameters represents the main problem for the theoretical analysis.

We start with one-dimensional problem which is relevant for sufficiently short laser pulses and nonfocused beams [1]. We write it in the moving reference frame fixed with the ablation front, and in terms of enthalpy per unit mass H:

$$\rho\frac{\partial H}{\partial t} = \rho v\frac{\partial H}{\partial z} + \frac{\partial}{\partial z}\left(\kappa\frac{\partial T}{\partial z}\right) - \frac{\partial I}{\partial z} \equiv B[T], \qquad (1)$$

where we introduced the notation B[T] for the right-hand side. The density of solid ρ is considered as constant, while the heat capacity c, heat conductivity κ, and the source term $(-\partial I/\partial z)$ may significantly depend on temperature T. The intensity I, within the solid shall obey Bouguer–Beer equation:

$$\frac{\partial I}{\partial z} = -\alpha I, \quad I|_{z=0} = I_s, \qquad (2)$$

where α is the absorption coefficient and I_s is the intensity absorbed at the surface. In some cases [1, 7], I_s can be related to laser pulse intensity $I_0 = I_0(t)$ by

$$I_s = I_0 A(T_s)\exp[-\alpha_g h], \qquad (3)$$

where A is the (temperature-dependent) absorptivity, and α_g is the vapor absorption coefficient, recalculated to the density of solid. The exponential term describes the shielding of radiation by the ablated material with thickness $h(t) = \int_0^t v(t_1)dt_1$. The surface evaporation (ablation) rate v is given by [7, 8]

$$v = v_0\exp\left[-\frac{T_a}{T_s}\right], \qquad (4)$$

where T_a is the activation temperature (in Kelvin), v_0 is preexponential factor (by the order of sound velocity), which can be considered as a constant.

The heat equation (1) should be solved together with boundary conditions. At the surface $z = 0$ it reads [7, 9]

$$\kappa\frac{\partial T}{\partial z}\bigg|_{z=0} = \rho v[L - H_s + H_{vs}]. \qquad (5)$$

Here, L is latent heat of vaporization and H_v and H are enthalpies of vapor and solid, respectively

$$H_v(T) = \int_{T_\infty}^{T} c_p(T_1)dT_1, \quad H(T) = \int_{T_\infty}^{T} c(T_1)dT_1, \qquad (6)$$

where c_p and c are the heat capacities for vapor and solid, and T_∞ initial temperature. Index s indicates the surface value, i.e., $H_{vs} = H_v(T_s)$, $H_s = H(T_s)$, etc.

The second boundary condition $T(z \longrightarrow \infty) \longrightarrow T_\infty$ and initial condition $T(t = 0) = T_\infty$ are trivial.

Using the second relation (6) between H and T the boundary condition (5) can be rewritten for the value of surface enthalpy gradient:

$$\frac{\partial H}{\partial z}\bigg|_{z=0} = \frac{v}{D_s}(L - H_s + H_{vs}) \equiv J_s. \qquad (7)$$

Here, $D = \kappa/c\rho$ is thermal diffusivity, $D_s = D(T_s)$, and we introduced the notation J_s for brevity.

Though somewhat simplified [7, 9], this model is still acceptable for the *quantitative analysis* of experimental data. In the present form it contains nonlinearities and nonstationary effects which can be analyzed by numerical solution with the help of finite-element technique (see e.g., [2]). This analysis requires big computational time and is not flexible. With the moment technique [10] which we will use in the further analysis,

this problem can be reduced to three coupled nonlinear *ordinary differential equations* with a small loss in accuracy. These equations can be solved by fast Runge–Kutta algorithms which are a routine part of many computational packages. Therefore, we obtain a fast tool for the quantitative simulation of thermal effects in laser ablation.

3. MOMENTS METHOD

The idea of "moments method" or "nonstationary averaging" method (see, e.g., [10]) is close to Galerkin method for approximate solution of nonlinear problems. This technique, was successfully applied, e.g., to problems in laser thermochemistry [11]. Here, we apply this technique for the analysis of laser ablation. The details of the procedure and the validation of the method's accuracy will be discussed elsewhere [12].

The idea of the method is simple. The exact solution of the boundary-value problem (1)–(6) fulfills (1) identically. If we use some approximate trial solution $H = H_p(z, t)$ the identity (1) will be violated and will result in the residue R:

$$\rho\frac{\partial H_p}{\partial t} - B[T_p] \equiv R[H_p]. \tag{8}$$

Nevertheless, we can use $H_p(z, t)$ as an approximate solution, if we demand that it fulfills the "conservation laws" for the moments M_n:

$$\frac{dM_n}{dt} - \int_0^\infty z^n B[T(H_p(z,t))]dz = 0,$$
$$\text{where } M_n = \int_0^\infty z^n H_p(z,t)dz. \tag{9}$$

The total number of equations (9) should be equal to the total number of unknown time-dependent functions which characterize $H_p(z, t)$. Equations (9) minimize residue R along the directions z^n within the functional space.

The difference between the Galerkin and moment methods refers to physics. There is no general algorithm for the choice of the trial function. The Galerkin method varies the trial functions in such a way that their combination is as close as possible to the "true solution." Some conservation law may not be fulfilled during the procedure. The moments method suggests less efficient approximation to the true solution, but it warrants that during the evolution certain conservation laws hold. As a result, the set of equations produced by the moment method usually has a clear physical sense.

For example, in (9), the equation for M_0 reflects the time-dependent energy balance, while equation for M_1 reflects the local energy balance with respect to some characteristic length.

We will consider two time-dependent parameters—surface temperature $T_s(t)$ (and associated surface enthalpy $H_s \equiv H[T_s(t)]$) and characteristic length $l(t)$ for the enthalpy distribution. These two quantities yield the most important information about the *distribution of internal energy* within the solid, which, as we believe, governs the ablation process. According to (9) we introduce two moments of *enthalpy* distribution:

$$M_0(t) = \int_0^\infty H(z,t)dz,$$
$$\text{and } M_1(t) = \int_0^\infty zH(z,t)dz. \tag{10}$$

Integration of equation (10) with (5) yields

$$\rho\frac{dM_0}{dt} = -\rho v H_s - \rho v[L - H_{vs} + H_s] + I_s, \tag{11}$$

and

$$\rho\frac{dM_1}{dt} = -\rho v M_0 + \int_{T_\infty}^{T_s(t)} \kappa(T)dT + \frac{I_s}{\alpha}. \tag{12}$$

The integral in the right-hand side is typical for the Kirchhoff transform [1]. We set the trial solution $H_p(z, t)$ in the following form:

$$H_p(z,t) = \frac{1}{1-\alpha l}[H_s + J_s l]\exp[-\alpha z]$$
$$-\frac{1}{1-\alpha l}[\alpha l H_s + J_s l]\exp\left[-\frac{z}{l}\right]. \tag{13}$$

This form satisfies boundary condition (13) and obvious requirement $H_p(z = 0, t) \equiv H_s(t)$. The first term in (13) describes the change of the enthalpy distribution with characteristic scale related to absorption of radiation, while the second term describes the changes related to heat conduction. From the physical point of view $l(t)$ represents the thermal length. Substitution of (13) into (10) yields

$$M_0 = (l + \alpha^{-1})H_s + \alpha^{-1} l J_s,$$
$$M_1 = (l^2 + l\alpha^{-1} + \alpha^{-2})H_s + (l + \alpha^{-1})\alpha^{-1} l J_s. \tag{14}$$

Now, we can substitute (14) into (11), (12) to obtain two ordinary differential equations for T_s and l. Note that J_s, as well as H_s, depends on surface temperature T_s via (7) and (6). It is not necessary to resolve the resulting equations with respect to dl/dt and dT_s/dt for the numerical computations which have been done with *Mathematica* software package [13].

The third equation for the thickness of ablated material [which we need for the description of the screening effect, see (3)] is given by

$$\frac{dh}{dt} = v. \tag{15}$$

Thus, the initial boundary-value problem is reduced to three ordinary differential equations for T_s, l, and h which should be solved with corresponding initial conditions. The study [12] shows, that this solution describes known analytical solutions with accuracy 5–10%. It also describes well the influence of the temperature-dependent $c(T)$, $\kappa(T)$, and $A(T)$ and, to a lower extent, $\alpha(T)$.

4. LASER ABLATION OF INDIUM: NUMERICAL SIMULATION

With laser ablation of metals one can often subdivide the fluences used in the ablation experiments into three regions:

(i) subthreshold ablation with $\Phi \ll \Phi_{th}$, where $\Delta h \propto \exp[-B/\Phi]$;

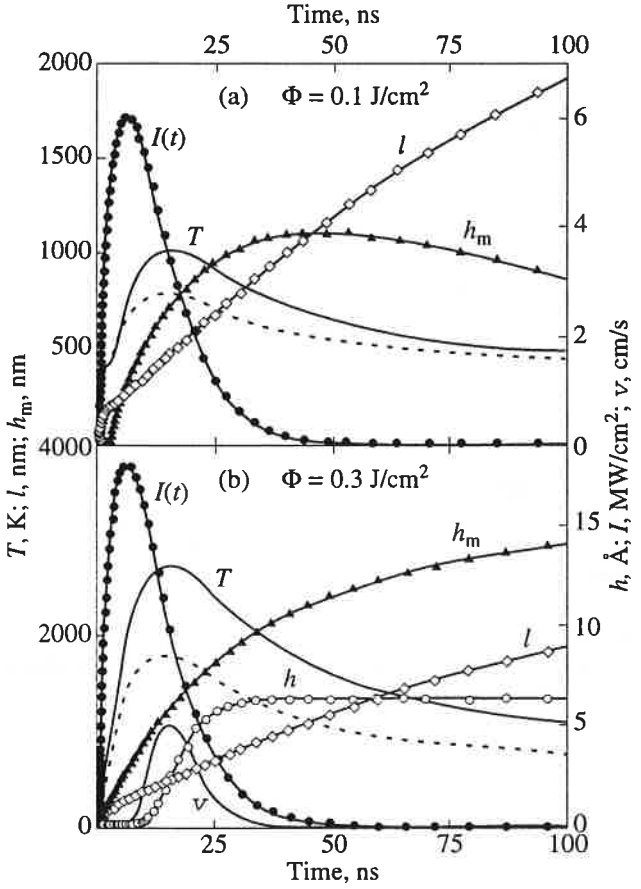

Fig. 1. Calculated dynamics of heating and ablation: (a) Φ = 100 mJ/cm^2 (subthreshold fluence) and (b) Φ = 300 mJ/cm^2. The surface temperature T_s (solid line), thermal length l (diamonds), and position of melt h_m (filled triangles) refer to the left axis, while the thickness of ablated material h (open circles), laser intensity I (filled circles), and the ablation velocity v (solid line) refer to the right axis. The temperature dependencies of $c(T)$, $\kappa(T)$, and $v(T)$ are given in the Appendix. The analytical temperature (18) is shown by dotted line. Initial temperature is T_∞ = 300 K. The value of absorptivity is A = 1, and the absorption coefficient is $\alpha = \alpha(T_\infty)$; t_{FWHM} = 15 ns.

(ii) near-threshold region with $\Phi \geq \Phi_{th}$, where $\Delta h \propto \Phi$;

(iii) region of developed ablation, $\Phi \geq (3\text{–}5)\Phi_{th}$, where the screening becomes important. For this region $\Delta h \propto \log[\Phi]$. An optical breakdown occurs at still higher fluences and highly ionized plasma forms near the target, which changes the ablation kinetics dramatically.

In the last two regions certain approximate solutions can be found [7, 14]. Above the threshold, the overall kinetics of thermal ablation is not very sensitive to nonstationary effects and material parameters. It is guided mainly by the overall energy conservation law and by the plasma properties at higher fluences. In this work we will be concerned with subthreshold ablation. Here ablation is essentially nonstationary and depends heavily on the material properties and pulse characteristics. This makes it difficult to write any approximate formulas for this region. To find ablated depth one has to calculate the integral

$$\Delta h = \int_0^{t \gg t_l} v(t)dt. \qquad (16)$$

This can be done easily with the help of moments method, the calculations with which can be carried out as fast as the calculations with approximate analytical formulas. The advantage of the moments method is also that we may describe with equal ease the experimental data in the intermediate situations, where no approximations exists.

We apply the developed method to the ablation of indium. The calculations are performed for KrF excimer laser (λ = 248 nm). Thermal and optical properties used in calculations are summarized in the Appendix. Indium has a low melting temperature, almost constant thermal conductivity, and the specific heat above the melting point. Ablation data have been measured for the background temperature below and above the melting point both for ns and fs laser pulses [61. This makes indium an attractive model system.

The hydrodynamic effects are weak for the ns pulses near the threshold. They can become more pronounced with higher fluences (higher recoil pressures) and multipulse irradiation [15–17]. In fact, developed hydrodynamic effects for ns laser pulse can be seen on the SEM photography, shown in [6]. Similar effects were found in ns experiments for bismuth and lead [15].

We approximate the temporal profile of the excimer laser pulse by a smooth function [1]

$$I(t) = I_0 \frac{t}{t_l} \exp\left[-\frac{t}{t_l}\right]. \qquad (17)$$

The laser fluence is given by $\Phi = I_0 t_l$. Note, that $t_l \approx 0.409 t_{FWHM}$ (the duration of the pulse defined at the full widths at half maximum). Below, this pulse is referred

to as "excimer" pulse. The analytical solution of the linear heat equation $T_{an}(t)$ presented for comparison in the first figure is given by

$$T_{an}(t) = T_\infty + \frac{\alpha}{\rho c}\int_0^t I(t-t_1)\exp[\alpha^2 D t_1]\operatorname{erfc}\sqrt{\alpha^2 D t_1}\,dt_1, \quad (18)$$

where parameters of the material are taken at $T = T_\infty$.

Figure 1 shows the *calculated* time dependencies of different quantities in a single ns pulse. In Fig. 1a ablation is absent, while in Fig. 1b several angstroms are ablated. The following features are worth noting.

(i) The rate of heating slows down near the melting point.

(ii) Melt exists extremely long after the end of the laser pulse ($\Delta t_m \gg t_l$). This is especially typical for indium with its low T_m and ΔH_m and high thermal conductivity, which allows one to melt a big volume. The flat tail in $T_s(t)$ dependence is due to the release of the latent heat of solidification.

(iii) The estimations of the surface temperature based on the analytical solution (18) of the heat equation may lead to big mistakes.

(iv) Ablation is *essentially* nonstationary. Ablation velocity is by no means constant during the pulse. Thermal length increases all the way during and after the pulse and is not very sensitive to the onset of ablation.

The last fact indicates that, for the parameters used here, ablation *cannot* be described by a quasi-stationary wave. It also suggests that the ablation threshold and rate may noticeably depend on the temporal profile and duration of the laser pulse.

Figure 2 demonstrates that the shape of the pulse influences the maximal temperature and the ablated depth significantly. This is due to the fact that with metals and ns laser pulses, T_{max} (near the threshold) is determined by heat conduction. This results in higher temperatures for more "compact" pulses, without tails, which lead to the unnecessary energy losses to the heating of material. The most compact pulse is the rectangular one. This is similar to the theoretical analysis [18], where it was shown, that the deepest melting (with fixed fluence and characteristic duration) is provided by the rectangular pulse. One can see that the ablation curves almost coincide for the rectangular pulse, and for the excimer pulse (17), with *twice* as small t_{FWHM} (dashed line). It is interesting to note that, although the maximal *temperature* for the short excimer pulse is slightly *lower*, the ablated *depth* is *higher*. Indeed, though the maximal ablation velocity is higher for the rectangular pulse, the effective width of the $v(t)$ is bigger for excimer pulse. As a result *integral* in (16) has higher value for a *smoother* excimer pulse.

With higher fluences the maximal temperature grows slower and the ablated depth becomes linear with

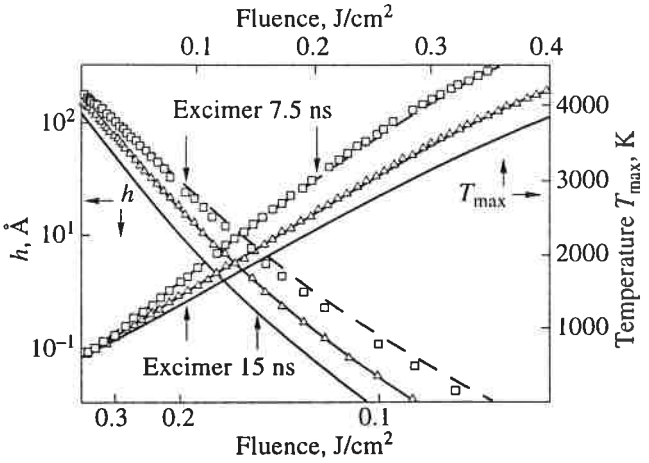

Fig. 2. The influence of the pulse shape onto the ablation. Three pulse shapes were used: rectangular, symmetric triangular, and smooth excimer pulse (17). Dashed lines refer to excimer pulse with t_{FWHM} = 7.5 ns. In all other cases t_{FWHM} = 15 ns. Initial temperature is T_∞ = 600 K. Other parameters are the same as in Fig. 1. The plots for the maximal temperature (right axis) vs. fluence (top axis) are shown in linear scale. The plot for the ablated thickness per pulse is shown in Arrhenius coordinates, i.e., log(h) (left axis) vs. inverse fluence $1/\Phi$ (bottom axis).

the fluence (as long as screening and hydrodynamics effects are negligible) due to latent heat of vaporization. The transition to this regime (which can be considered as an ablation threshold) occurs above Φ = 0.3 J/cm² when the amount of ablated material per pulse exceeds 100 Å. This threshold significantly depends on the pulse shape. Thus, with *the same* t_{FWHM} experiments can show *different* threshold fluences. It is important, for example, for excimer lasers, where the pulse shapes can vary strongly. We emphasized the importance of the temporal shape of the laser pulse previously [1, 18, 19].

Another interesting feature of Fig. 2 is that the "Arrhenius plot" $\log(h)$ versus $1/\Phi$ is *steeper* than linear below the Φ_{th}, in spite of the fact that the temperature *is linear* with fluence in this region. The slope of $\log(h)$ versus $1/\Phi$ dependence is influenced by the pulse shape and duration. The reason for this is again the widening of the temporal region with $v(t) \neq 0$ in the integral (16). For the analysis of the experimental data, one also has to have in mind that with many excimer lasers t_{FWHM} increases with the output pulse energy.

Figure 3 illustrates the influence of temperature dependences in $A(T)$ and $\alpha(T)$ onto ablation curves. As in Fig. 2, for simplicity calculations are performed for *liquid* indium. With ns pulses $\alpha^2 D t_l \gg 1$, and absorption is essentially surface. This holds even for smaller values of α at elevated temperatures (see the Appendix). As a result, $\alpha(T)$ dependence makes only a minor difference for ns pulses. The difference, which can be seen in the figure, is almost entirely due to $A(T)$ dependence, and is "accumulated" during the initial stage of heating,

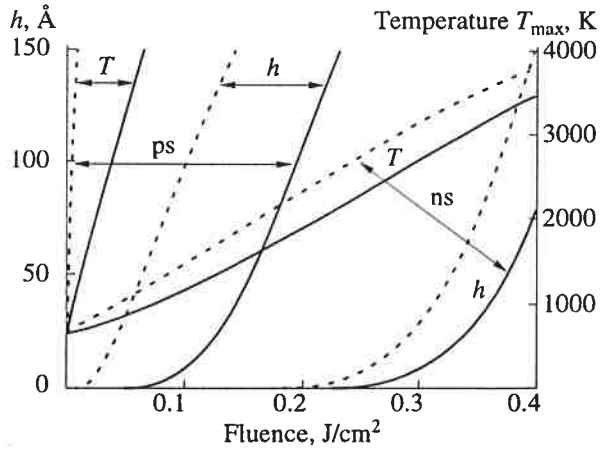

Fig. 3. The influence of temperature dependencies in A and α onto the ablation. For ns pulses the solid curves refer to the temperature-dependent coefficients. Dotted lines refer to $A = 1$. For ps pulses solid curves refer to $\alpha = 10^5$ cm^{-1}, while dotted lines, to $\alpha = 1.2 \times 10^6$ cm^{-1}. The absorptivity for ps pulses is $A = 1$. Initial temperature is $T_\infty = 600$ K in all cases. Other parameters are the same as in Fig. 1.

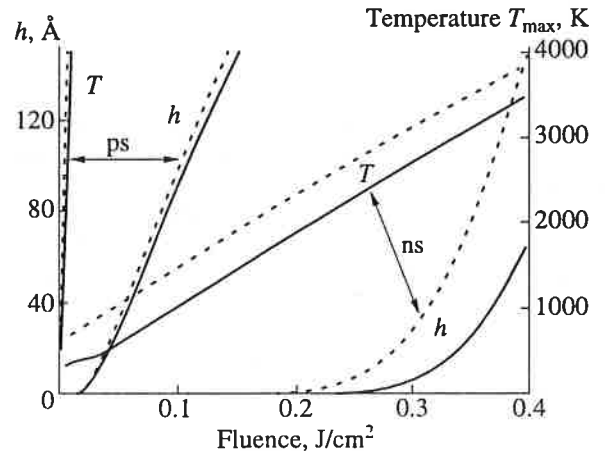

Fig. 4. The influence of the initial temperature T_∞ onto the ablation. Solid curves refer to $T_\infty = 300$ K and dotted curves, to $T_\infty = 600$ K. Absorptivity is $A = 1$, and the absorption coefficient is $\alpha = 1.2 \times 10^6$ cm^{-1} for all curves.

when the absorptivity is significantly smaller than one (A.7). One can also see a faster than linear increase in the T_{max} at low fluences, where absorptivity strongly increases with temperature.

The analysis of the ps pulses (with $\alpha^2 Dt_l \ll 1$) with the present model has a more qualitative character. Thermal *surface* evaporation model can be applied to ps pulses near and below the threshold only. This is related to several factors. According to [5], electron–phonon thermalization occurs within subpicosecond range. As a result, the temperatures much higher than the boiling temperature, and probably even the critical temperature T_k, are reached already at low fluences. This leads to the following complications.

(i) With temperature approaching T_k, the distinction between the condensed and the solid phase disappears. This results in the decrease in the vaporization enthalpy $\Delta H = L - H_{vs} + H_s$ (which is equal *zero* at the critical temperature). At the same time, specific heat tends to infinity at T_k [20]. Above T_k only one phase exists. The material does not have the time to fly out of the laser beam, and provides very strong screening even at relatively low temperatures. With high fluences, it is more realistic to assume simply that all material heated above T_k is ablated.

(ii) The moment method in its present form adopted for the brevity in this work yields rather big mistakes in the case of short pulses $\alpha^2 Dt_l \ll 1$, when α strongly changes with temperature [12].

(iii) Besides, optical parameters of indium at high temperatures are known only from the extrapolations.

For these reasons, we present in Fig. 3 the results for $A(T)$ and two constant values of α. Temperature dependence of absorptivity does not influence the ablation curves, because with ps pulses, already at low fluences the temperatures are so high that $A \approx 1$ [see (A.7)]. Dependence $\alpha(T)$, to the contrary, is very important. The maximal surface temperature is proportional to α in this region (calorimetric solution). This about triples ablation threshold when α is decreased from 1.2×10^6 to 10^5 cm^{-1}. The temperature for $\alpha(T)$ dependence given by (A.8) lies between the dotted and the solid curve, while the behavior of the ablated depth near the threshold is quite similar to that for $\alpha = 10^5$ cm^{-1}, due to high temperatures achieved in this region.

Thus, high-temperature behavior of the absorption coefficient (which is usually *not* known from the direct measurements) is extremely important for the determination of ablation threshold in the ps pulses, and unimportant in the ns case. The $A(T)$ dependence, to the contrary, influences the ns threshold, but not the ps one.

Figure 4 shows the influence of the ambient temperature onto the ablation curves. With ns pulses, the main difference stems from two factors:

(i) Thermal conductivity of liquid phase is about twice as small as for the solid indium. This yields a reduction in the slope in initial part of $T(\Phi)$ dependence for $T_\infty = 600$ K.

(ii) The necessity to heat over 300 more Kelvin when heating starts from $T_\infty = 300$ K. The heat of fusion is anomalously small for indium and is less important than these factors.

The fluences necessary for the developed ablation from solid and liquid phases differ by some 20–25%. The relative difference becomes more pronounced for very small ablated depths.

This is not the case with ps pulses, where the curves for the temperature and the ablated depth almost coincide for both T_∞. The reason is that, with ps pulses, due

Table

Parameter	Value	Units
Atomic number, A	49	
Atomic weight, M	114.76	g/mole
Density, ρ	7.3	g/cm^3
Melting temperature, T_m	430	K
Vaporization (boiling) temperature, T_v (corresponds to saturated vapor pressure P = 1 atm.)	2340	K
Latent heat of fusion, ΔH_m	28.5	J/g
Latent heat of vaporization, ΔH_v	1960	J/g
The Debye temperature, T_D	108	K

to their short duration, ablated depth comparable to that of ns pulses is achieved at higher ablation velocities, that is, at higher temperatures. In this case 300 K difference in the background temperature is less important. Besides, the heat conduction plays less important role in ps pulses. It determines the cooling time of the surface, i.e., enters the ablated depth almost linearly. In ns pulses, it determines the maximal temperature, and as a result exponentially influences the ablated depth.

Thus, we should consider that laser ablation of indium with nanosecond pulses seems to be purely thermal although the temperature dependencies of material parameters strongly influence ablation rate. On the contrary, with subpicosecond pulses some other effects (not included into the discussed model) play an important role.

Effects related to the difference in electron and lattice temperature [21][1] seem to be the most important as well as the critical phenomena (heating above the critical temperature).

5. CONCLUSIONS

Numerical simulations of nonstationary effects in thermal surface laser ablation of indium are performed on the basis of the nonstationary averaging technique. Nonstationary effects influence the kinetics of laser ablation differently for nanosecond and picosecond laser pulses. Below we summarize the results.

– There exists a big difference in characteristic temperatures during the ablation by ns and ps pulses. For ps pulses temperatures are significantly higher and probably exceed critical temperature. This may render surface ablation model irrelevant already near the ablation threshold.

– Experimentally measured ablation threshold for ps pulses [6] is significantly higher than expected from the data based on room temperature values of absorption coefficient. This is probably due to a significant decrease in absorption coefficient with temperature.

– There exists a big difference in the ablation rates for ns ablation of solid and liquid indium, while for ps pulses this difference is practically absent.

– With indium, the kinetics of ablation with ns pulses is sensitive to the nonlinearities caused by the temperature dependencies in thermal conductivity and absorptivity. At the same time it is not sensitive to temperature dependence in absorption coefficient. With ps pulses, only the temperature dependence in the absorption coefficient strongly influences kinetics.

– Ablation threshold and near-threshold kinetics of nanosecond laser ablation (unlike the picosecond one) are sensitive to the temporal shape of laser pulse. Subthreshold ablated depth may deviate from the Arrhenius dependence on fluence due to nonstationary effects, and the slope of this Arrhenius dependence depends noticeably on the pulse shape.

ACKNOWLEDGMENTS

The authors are grateful to the Russian Foundation for Basic Research and the "Fonds zur Forderung der wissenschaftlichen Forschung in Osterreich" for financial support.

APPENDIX: THERMOPHYSICAL AND OPTICAL PROPERTIES OF INDIUM

(a) The table summarizes the parameters of indium which were taken as constant in calculations. The data were taken from [22, 23].

(b) Specific heat $c(T)$. The algorithm uses the analytical integration for the enthalpy. Thus, the specific heat (as well as the thermal conductivity) was fitted by the functions which allow analytical integration. The coefficients were found by the minimization of

[1] We should mention that the moments technique was used in [21] to estimate ablated layer thickness under simplified assumptions (one-temperature approximation with constant material parameters).

least-square deviation. The interpolation holds within 250–3000 K. $c(T)$ is measured in J/g K and T, in K,

$$c_p(T) = 0.25 + 1.19\times10^{-2}\arctan\left[\frac{T-T_m}{\Delta T}\right] - 1.49\times10^{-5}T\arctan\left[\frac{T-T_m}{\Delta T}\right], \quad (A.1)$$

The temperature width of melting $\Delta T = 0.01T_m \approx 43$ K was introduced to smoothen steplike changes in parameters near T_m. The constant specific heat approximation with $c_p \approx 0.24$ J/gK results in less than 4% difference in the calculated temperature, and can be used as well. The Debye interpolation formula [20], as well as the Dulong–Petit law, deviates from the experimental data. These deviations are probably caused by anharmonicity.

The latent heat of fusion was taken into account by the "specific heat of melting" which was written in a Lorentzian form

$$c_m(T) = \frac{\Delta H_m}{\pi}\frac{\Delta T}{\Delta T^2 + (T-T_m)^2}. \quad (A.2)$$

The total specific heat is given by

$$c(T) = c_p(T) + c_m(T). \quad (A.3)$$

(c) Thermal conductivity $\kappa(T)$. The interpolation formula was taken in the form

$$\kappa(T) = 0.396 - 0.23\left(\arctan\left[\frac{T-T_m}{\Delta T}\right] - \frac{\pi}{2}\right) + 2.6\times10^{-4}T\left(\arctan\left[\frac{T-T_m}{\Delta T}\right] - \frac{\pi}{2}\right). \quad (A.4)$$

It includes jump at the melting temperature and fits experimental data [23, 24] with sufficient accuracy within the region from 250–3000 K.

(d) Surface evaporation rate. According to [22],the evaporation rate is given by

$$v(T) = v_1\sqrt{\frac{300}{T}}\exp\left[-\frac{T_a}{T}\right], \quad (A.5)$$

where $T_a = 28000$ K and $v_1 = 4.2\times10^5$ cm/s. Without loss of accuracy the value $v_0 = 1.5\times10^5$ can be used in (4) for the whole preexponential factor (its value at boiling temperature). The activation energy is in agreement with measurements on saturated vapor pressure, which yields $T_a = 29000$ K [22].

(e) Optical properties of indium. The data given in [22] yield too high value of $A \sim 0.4$–0.6. The ideal films of indium prepared in ultrahigh vacuum conditions and well annealed show a big reflectivity (see [25, 26]). Using Drude theory we extrapolate data [23] for 298 K to the wavelength of KrF excimer laser ($\lambda = 248$ nm, $\hbar\omega = 5$ eV). It yields $A = 0.16$ for the absorptivity and $\alpha = 1.2\times10^6$ cm^{-1} for the absorption coefficient.

We use the Drude formulas for the calculation of the temperature dependencies and the relation $\sigma(T)T = \text{const}$ which should be fulfilled above the Debye temperature [27]. We assume that this approximation holds for indium above 300 K.

To find the jump in the optical characteristics at melting temperature we can use the continuity of the Wiedemann–Franz ratio $\kappa(T)/T\sigma(T)$ across the melting point [24]:

$$\left.\frac{\sigma_s}{\sigma_l}\right|_{T=T_m} = \left.\frac{\kappa_s}{\kappa_l}\right|_{T=T_m} = 2.1. \quad (A.6)$$

This yields jump in absorptivity up to $A \approx 0.4$ at melting temperature. For the smooth interpolation of absorptivity above the melting temperature we used

$$A(T) = 1 - 0.6\exp\left[\frac{T_m - T}{1200}\right]. \quad (A.7)$$

The jump in α is small and almost does not influence the heating. It was not included in the interpolation which we used:

$$\alpha(T) = \frac{10^6}{\alpha_0 + \alpha_1 T}[\text{cm}^{-1}], \quad (A.8)$$

where $\alpha_0 = 0.582$, $\alpha_1 = 7.813\times10^{-4}$.

REFERENCES

1. Bäuerle, D., 1996, *Laser Processing and Chemistry*, 2nd ed. (Berlin: Springer).
2. 1996, *Laser Ablation*, Fogarassy, E., Geohegan, D., and Stuke, M., Eds. (Amsterdam: North-Holland).
3. 1992, *Laser Ablation of Electronic Materials*, Fogarassy, E. and Lazare, S., Eds. (Amsterdam: North-Holland).
4. Gaponov, S.V., 1985, *Sov. Phys. Uspekhi*, **28**, 522.
5. Anisimov, S.I. and Khokhlov, V.A., 1995, *Instabilities in Laser–Matter Interaction* (Boca Raton: CRC).
6. Preuss, S., Demchuk, A., and Stuke, M., 1995, *Appl. Phys. A*, **61**, 33.
7. Anisimov, S.I., Imas, Ya.A., Romanov, G.S., and Khodyko, Yu.V., 1971, *Action of High-Power Radiation on Metals* (Springfield, VA: National Technical Information Service).
8. Sobol, E.N., 1995, *Phase Transformations and Ablation in Laser-Treated Solids* (New York: John Wiley).
9. Luk'yanchuk, B., Bityurin, N., Himmelbauer, M., and Arnold, N., 1997, *Nucl. Instrum. Meth. B*, **122**, 347.
10. Zwillinger, D., 1989, *Handbook of Differential Equations*, (Boston: Academic).
11. Karlov, N.V., Kirichenko, N.A., and Luk'yanchuk, B.S., 1997, *Laser Thermochemistry*, 2nd ed., (Cambridge Interscience Press).
12. Arnold, N., Luk'yanchuk, B., and Bityrin, N., 1998, *Appl. Surf. Sci.* (in press).
13. Wolfram, S., 1991, *Mathematica*, 2nd ed., (Addison-Wesley).

14. Tokarev, V.N., Lunney, J.G., Marine, W., and Sentis, M., 1995, *J. Appl. Phys.*, **78**, 1241.
15. Vedenov, A.A., and Gladush, G.G., 1985, *Physical Processes in Laser-Treated Materials*, (Moscow: Energoatomizdat) (in Russian).
16. Yth, C.S., 1974, *Phys. Fluids*, **14**, 1936.
17. H. Ven, Shui, 1978, *Phys. Fluids*, **21**, 2174.
18. Bunkin, F.V., Kirichenko, N.A., and Luk'yanchuk, B.S., 1978, *Preprint Lebedev Physical Institute*, no. 146, Moscow, USSR; 1980, *Fiz. Khim. Obrabotki Materialov*, **5**, 7.
19. Luk'yanchuk, B., Bityurin, N., Anisimov, S., *et al.*, 1996, *Appl. Phys. A*, **62**, 397.
20. Landau, L.D. and Lifshitz, E.M., 1980, *Statistical Physics*, (Pergamon), part 1.
21. Anisimov, S.I. and Rethfeld, B., 1997, *Proc. SPIE*, **3093**, 192.
22. 1973, *American Institute of Physics Handbook*, 3rd ed., Gray, D.E., Ed. (Mc Graw-Hill).
23. 1980, *Landolt-Bornstein New Series*, Madelung, O. Ed. (Berlin: Springer).
24. Goldratt, E. and Greenfield, A.J., 1980, *J. Phys. F*, **10**, 295.
25. Koyama, R.Y., Smith, N.V., and Spicer, W.E., 1973, *Phys. Rev. B*, **8**, 2426.
26. Lemonuier, J.C., Jezequel, G., and Thomas, J., 1975, *J. Phys. C*, **8**, 2818.
27. Lifshitz, E.M. and Pitaevsky, L.P., 1981, *Physical Kinetics*, (Pergamon).